Nanoscale Advances

ROYAL SOCIETY OF CHEMISTRY

PAPER

View Article Online
View Journal | View Issue

Cite this: *Nanoscale Adv.*, 2025, **7**, 7579

Corrosion behavior of anodized nanoporous TiO_2 films in oxidizing environments: a study on electrochemically engineered titanium surfaces

Surya Prakash Gajagouni, *[ab] Imad Barsoum,[ab] Sung Oh Cho [c] and Akram Alfantazi[bd]

This study presents a systematic investigation into the fabrication and corrosion behavior of nanoporous titanium dioxide (TiO_2) films formed *via* electrochemical anodization. Optimized anodization parameters, including electrolyte composition, applied voltage, and processing duration, yielded uniform nanoporous TiO_2 layers with pore diameters of 60–70 nm and thicknesses of 2–3 μm. Structural and compositional analyses using SEM, EDS, and XRD confirmed the formation of a well-ordered anatase TiO_2 phase. Post-anodization annealing further enhanced oxide purity by eliminating residual fluorides, as evidenced by XPS depth profiling. Electrochemical characterization in 25 mM Na_2SO_4 with increasing H_2O_2 concentrations revealed significantly improved corrosion resistance of anodized Ti compared to untreated Ti. Despite the lower polarization resistance (R_p) observed in EIS, the anodized oxide exhibited stable passivation, reduced corrosion current densities, and favorable capacitive behavior, attributed to its porous morphology and chemical stability. These findings demonstrate that engineered nanoporous TiO_2 films offer robust corrosion protection in oxidizing environments, supporting their application in biomedical devices, catalytic systems, and advanced nuclear materials.

Received 15th September 2025
Accepted 19th September 2025

DOI: 10.1039/d5na00883b

rsc.li/nanoscale-advances

Introduction

Nanoporous titanium dioxide (TiO_2) structures have attracted considerable attention due to their unique physicochemical properties, including high surface area, tunable pore architecture, and excellent chemical stability. These features make them promising candidates for a broad range of applications, such as photocatalysis, biomedical implants, sensors, and protective surface coatings.[1–4] Electrochemical anodization is widely recognized among various fabrication methods for its simplicity, scalability, and precise control over pore size, oxide thickness, and morphology. The anodization process involves applying a controlled potential in a suitable electrolyte, leading to the self-organized growth of porous or tubular oxide layers on the titanium substrate. The resulting structure and properties of the oxide layer are strongly influenced by parameters such as electrolyte composition, water content, applied voltage, temperature, and anodization duration.[5,6] By tailoring these conditions, nanoporous TiO_2 layers with desired dimensions and crystallinity can be achieved to suit specific application needs.[7,8]

While the anodization of Ti for photocatalytic and biomedical applications has been extensively studied, relatively fewer investigations have focused on the corrosion resistance and electrochemical stability of these nanoporous oxides in aggressive environments.[9,10] Titanium naturally forms a passive oxide film that offers inherent corrosion protection; however, this native film may deteriorate under oxidative stress, particularly in the presence of reactive oxygen species such as hydrogen peroxide (H_2O_2). Optimized anodized oxide layers, especially after post-treatment such as annealing, may offer superior chemical stability, structural integrity, and resistance to dissolution.[11,12] Understanding the corrosion behaviour of anodized TiO_2 layers under oxidizing conditions is critical for advanced applications, particularly in biomedical, catalytic, and nuclear environments where materials are subjected to long-term oxidative stress.[13] In this context, H_2O_2 is a representative oxidizing agent for simulating harsh aqueous environments.[14] Studying the oxide's response to varying concentrations of H_2O_2 provides valuable insights into its passivation, stability, and protective performance.[15,16]

This study aims to develop uniform, crystalline nanoporous TiO_2 layers through controlled anodization and annealing to enhance oxide purity and phase stability. The corrosion behaviour of these surfaces is systematically evaluated in neutral sulphate electrolytes containing different

[a]*Department of Mechanical and Nuclear Engineering, Khalifa University, Abu Dhabi 127788, United Arab Emirates. E-mail: surya.goud28@gmail.com*

[b]*Emirates Nuclear Technology Center (ENTC), Khalifa University, Abu Dhabi 127788, United Arab Emirates*

[c]*Department of Nuclear and Quantum Engineering, Korea Advanced Institute of Science and Technology (KAIST), Daejeon 34141, South Korea*

[d]*Department of Chemical and Petroleum Engineering, Khalifa University, Abu Dhabi 127788, United Arab Emirates*

concentrations of H_2O_2. Electrochemical techniques correlate the oxide structure with corrosion performance, including open circuit potential monitoring, potentiodynamic polarization, and impedance spectroscopy. The findings offer critical guidance for designing durable Ti-based surfaces for high-performance and oxidative environments.

Experimental

Sample preparation

Commercially pure titanium (>99.95%) sheets were 1 mm thick and cut into 10 × 15 mm^2 specimens. The samples were ultrasonically cleaned in acetone, ethanol, and deionized water for 15 min each and subsequently dried with hot compressed air. Electropolishing was carried out in 20–25% $HClO_4$ in ethylene glycol monobutyl ether at 30 V for 5–10 min in an ice bath maintained below 5 °C. After rinsing and drying, anodization was performed at 60–70 V for 15 min in an electrolyte containing 0.1 M NH_4F and 0.1 M H_2O in ethylene glycol, using a platinum spring as the counter electrode. Following anodization, the samples were rinsed in ethanol and annealed at 450 °C for 90 min to promote crystallization of the oxide layer.

Characterization

Surface morphology was examined using a field-emission scanning electron microscope (Quanta 3D FEG – SEM/FIB, Thermo Fisher Scientific) equipped with a silicon drift detector (SDD) for energy dispersive spectroscopy (EDS) analysis of elemental composition. Phase identification of the oxide layers was performed using X-ray diffraction (Empyrean, Malvern PANalytical). Surface chemistry and depth profiling were studied by X-ray photoelectron spectroscopy (XPS, ESCALAB Xi^+, Thermo Fisher Scientific) using a monochromatic Al Kα source.

Electrochemical studies

Electrochemical measurements were carried out at room temperature using a Gamry potentiostat in a conventional three-electrode configuration, with the bare and anodized titanium specimens as working electrodes, a platinum wire as the counter electrode, and an Ag/AgCl (saturated KCl) electrode as the reference electrode. The open-circuit potential (OCP) was monitored continuously from immersion in 25 mM Na_2SO_4 with 0–0.1 M H_2O_2. Samples were left to stabilize for ~30 min, after which OCP readings were recorded until the potential drift was less than 0.1 mV per min over a 10 min period (typically achieved within additional 10–20 min). Fresh H_2O_2 solutions were prepared for each test and protected from light to minimize decomposition.

Potentiodynamic polarization (linear sweep voltammetry, LSV) was performed from −0.5 V to +2.0 V (*vs.* Ag/AgCl) at a scan rate of 1 mV s^{-1}. Corrosion parameters, including the corrosion potential (E_{corr}), corrosion current density (I_{corr}), and anodic/cathodic Tafel slopes (β_a/β_c), were obtained by Tafel extrapolation from the linear portions of the polarization curves. Electrochemical impedance spectroscopy (EIS) was conducted at the OCP in the frequency range of 100 kHz to 10 mHz with a 10 mV rms AC perturbation.

Results and discussion

During electrochemical anodization, nanoporous TiO_2 forms through a dynamic competition between oxide growth at the metal–oxide interface and localized dissolution at the oxide–electrolyte interface. Under an applied electric field, titanium oxidizes to Ti^{4+}, which reacts with O^{2-} or OH^- to form a compact oxide. In fluoride-containing electrolytes, the electric field promotes the dissolution of this oxide by forming soluble [Ti–F] complexes at the oxide–electrolyte interface. This field-assisted dissolution, occurring simultaneously with continuous oxide growth, initiates pore formation. Over time, a self-organized structure develops due to the balance between vertical oxide formation and localized dissolution at the pore bases, resulting in a uniform nanoporous morphology.[2,17]

The evolution of titanium's surface morphology during anodization was systematically studied using an electrolyte of 0.1 M NH_4F and 0.1 M DI water in ethylene glycol, under an applied potential of 70 V for 15 min. The process was conducted at temperatures maintained below 5 °C using an ice bath to ensure

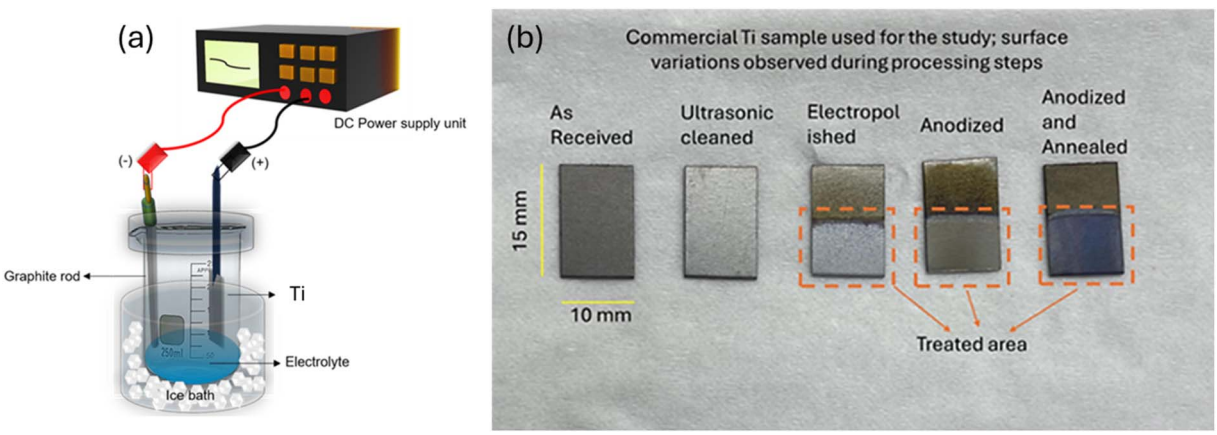

Fig. 1 Schematic of the electrochemical cell setup used for electropolishing and anodization. (a) A 100 ml beaker filled half with electrolyte, graphite as the counter electrode, and a titanium working electrode. (b) Commercially pure titanium samples, optical images showing surface color variations at different stages during the anodization process.

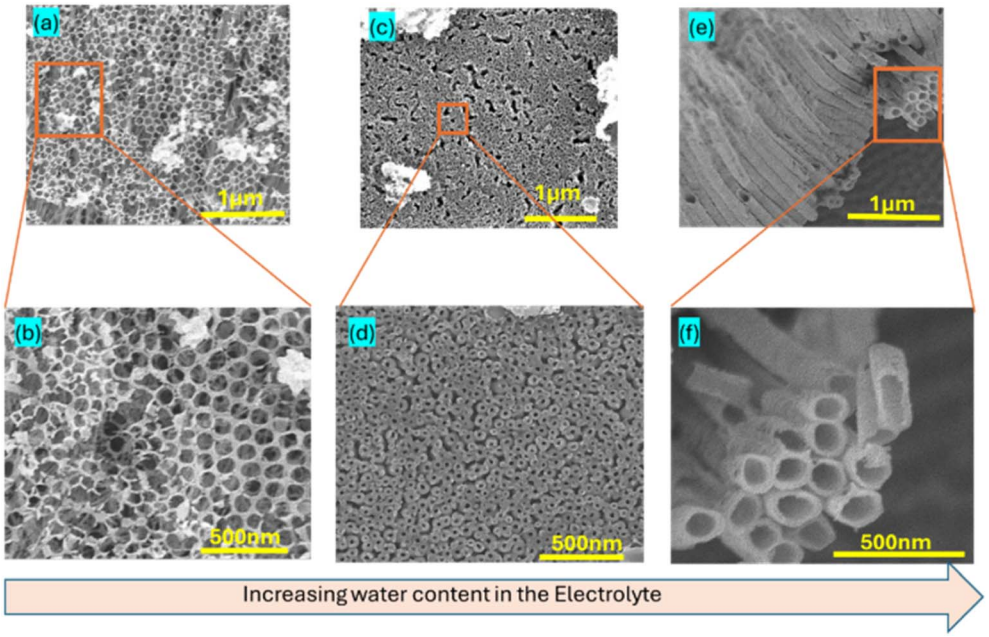

Fig. 2 SEM images of anodized Ti at different water contents in the electrolyte (0.1 M NH_4F in ethylene glycol, 70 V, and 15 min). Low- and high-magnification images illustrate the morphological transition from pores to tubes: (a and b) 0.05 M H_2O, (c and d) 0.1 M H_2O, and (e and f) 0.2 M H_2O. Uniform pore diameters of 60–70 nm were obtained at 0.1 M H_2O.

controlled reaction kinetics. This optimized process resulted in forming a nanoporous titanium dioxide (TiO_2) layer with a uniform pore size of 60–70 nm and a thickness of approximately 2–3 μm. These morphological characteristics are critical for various applications, including enhanced corrosion resistance, catalysis, and biomedical coatings. As shown in Fig. 1, variations in the surface color of the Ti sample were observed during anodization at various stages.[17] The controlled conditions, particularly the low temperature and fluoride content in the electrolyte, facilitated the formation of well-defined and evenly distributed nanopores.[18,19]

Effect of water content on surface morphology

SEM images demonstrate the impact of water content in the anodization electrolyte on the resulting surface morphology. At a water concentration of 0.1 M, the oxide layer displayed highly uniform pore sizes (60–70 nm) and a consistent thickness (~2–3 μm). This consistency suggests that the selected electrolyte composition was optimized for an ordered and stable nanostructure. As shown in Fig. 2 and S3, the pore morphology transitions to nanotubes with increasing water content in the electrolyte containing 0.1 M NH_4F in ethylene glycol while maintaining the voltage constant at 70 V for 15 min.[3] This behavior is attributed to enhanced field-assisted dissolution and the role of water in oxygen ion transport, both of which affect pore wall thinning and inter-pore merging. These results confirm that electrolyte water concentration is a key parameter in tailoring nanoporous *versus* nanotubular TiO_2 architectures.[14,20,21]

Influence of voltage on surface morphology

The applied voltage significantly influences the anodization process, as evidenced by SEM images. At 70 V, the anodized titanium exhibited a highly ordered nanoporous structure. Higher voltages are expected to enhance the electric field strength, accelerate oxide formation, and potentially affect the pore size and distribution. The stability and order observed at 70 V highlight the effectiveness of this condition in forming a robust oxide layer. As shown in Fig. 3, studies examining SEM images at various voltages reveal melting or thinning of pore walls at higher voltages, likely due to increased Joule heating and ion mobility. These changes point to localized dissolution, which may compromise oxide stability. Further chemical analysis of the anodized surfaces is necessary to clarify the interplay between the voltage, oxide structure, and pore wall integrity.[22]

XRD analysis: phase evolution and stability

X-ray diffraction (XRD) analysis was conducted to investigate the phase composition and crystallinity of the oxide layers formed on the Ti surface before and after anodization, as well as after exposure to corrosive media. As illustrated in Fig. 4, the diffraction pattern of bare Ti displays prominent peaks corresponding to the hexagonal close-packed (hcp) α-Ti phase. Following anodization, additional peaks emerge, which match well with the anatase phase of TiO_2. The presence of anatase indicates partial crystallization of the anodic oxide, likely promoted by localized heating during anodization or subsequent thermal treatment. After immersion in a 25 mM Na_2SO_4 solution, the anatase peaks remain visible, suggesting structural integrity and resistance to dissolution in neutral media. Interestingly, exposure to 25 mM Na_2SO_4 + 0.1 M H_2O_2 increases the intensity of anatase peaks. This enhancement indicates either an improved crystalline layer of the oxide layer or increased

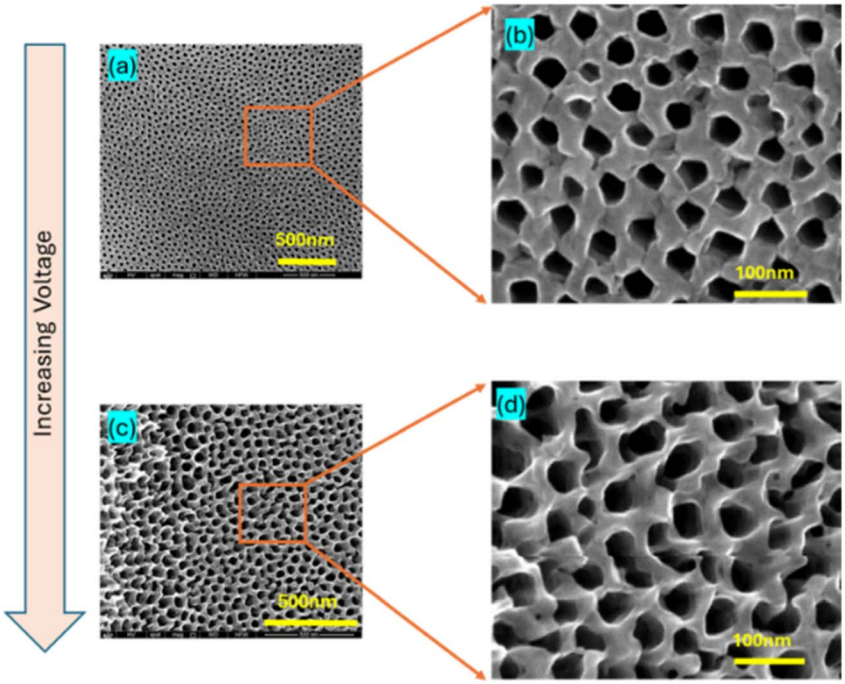

Fig. 3 SEM images of anodized Ti at varying anodization voltages in 0.1 M NH_4F + 0.1 M H_2O in ethylene glycol. (a and b) At 70 V, showing well-ordered pores; (c and d) at 80 V, showing pore wall thinning and localized dissolution effects. Images are presented at low (a and c) and high (b and d) magnifications.

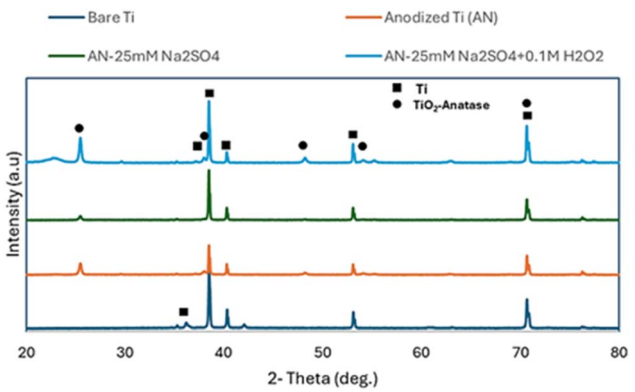

Fig. 4 XRD diffraction patterns of bare Ti, anodized Ti, and anodized Ti after corrosion studies in 25 mM Na_2SO_4 without and with 0.01 M H_2O_2. The anatase TiO_2 phase is visible after anodization and becomes more prominent after corrosion in oxidizing environments, demonstrating structural stability and enhanced oxide crystallinity.

exposure of crystalline domains at the surface due to selective dissolution of amorphous regions. The retention and enhancement of the anatase phase in oxidizing media highlight its stability and potential functional benefits, such as increased corrosion resistance and photocatalytic activity.[17]

Elemental composition of the anodized layer (EDS and XPS analyses)

The surface morphology and elemental composition of the anodized Ti samples were examined using SEM coupled with EDS analysis. SEM imaging (Fig. S1) revealed a uniform feather-like or nanograss-like surface morphology, characteristic of TiO_2 structures formed *via* anodization in fluoride-containing electrolytes. These features suggest the development of a porous, high-surface-area oxide film, which is beneficial for applications requiring surface reactivity, such as catalysis and biomedical coatings. EDS spectra confirm the presence of titanium and oxygen, with atomic percentages of approximately 33.4% and 64.8%, respectively, consistent with the expected stoichiometry of TiO_2. The detected carbon is attributed to surface contamination from ambient exposure and cleaning reagents. Elemental mapping over the analyzed region showed a homogeneous distribution of Ti and O, affirming the uniformity of the anodic oxide. These findings validate the success of the anodization process in producing a well-distributed, chemically consistent oxide layer.[23,24]

XPS was performed on both anodized and anodized–annealed Ti to further assess the surface chemistry and elemental distribution. The anodized Ti surface's survey spectra (Fig. 5a) revealed Ti 2p and O 1s peaks, along with F 1s, C 1s, and minor N 1s signals. The presence of fluorine is attributed to incorporation during anodization in fluoride-containing electrolytes, while carbon and nitrogen arise from surface contamination. However, the anodized–annealed sample showed a marked reduction in F 1s and C 1s intensities, along with an increase in Ti and O peaks, indicating successful removal of fluorine species and surface contaminants during annealing.[25]

Depth profile analysis (Fig. 5b) further demonstrated the compositional transformation induced by annealing. In anodized Ti, the F concentration increased with depth (~10.4% at

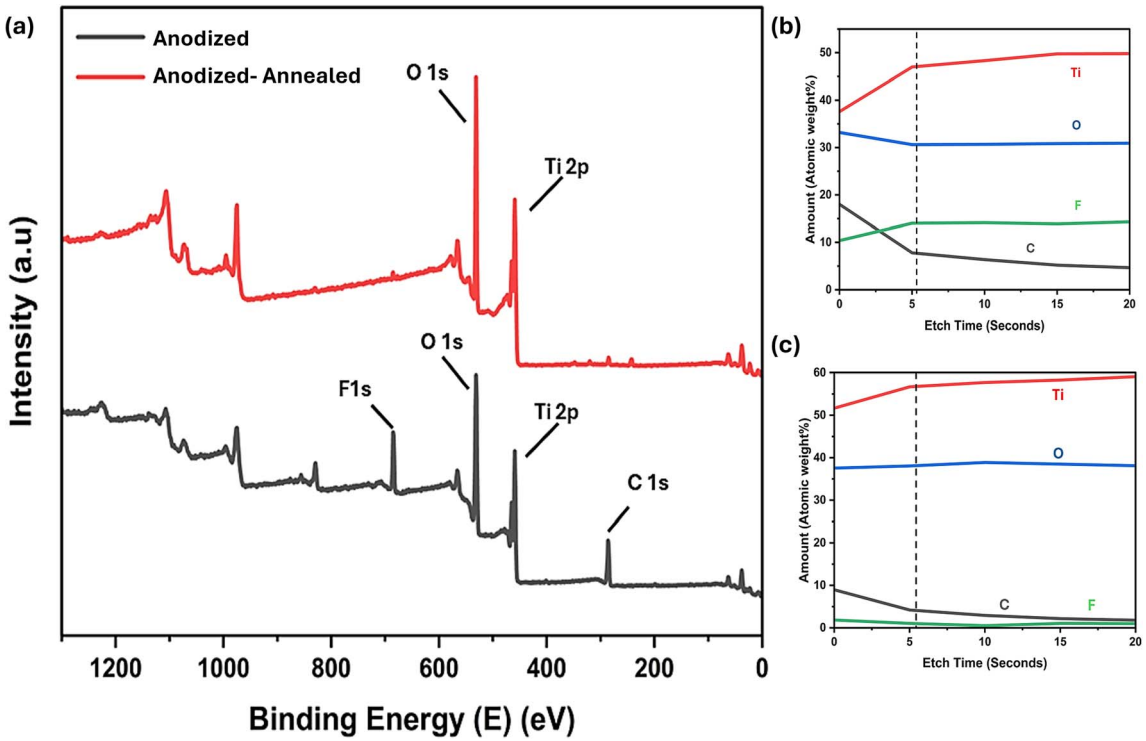

Fig. 5 XPS analysis of anodized and annealed Ti: (a) survey spectra showing Ti 2p, O 1s, F 1s, and C 1s signals; (b and c) depth profiling of anodized and annealed Ti, highlighting compositional changes with etching time. Annealing results in a significant reduction of fluorine and carbon contamination and enrichment of Ti and O, indicating oxide densification and chemical stabilization.

the surface to ~14.3% at 20 s), while Ti and O signals stabilized around 49.8% and 31%, respectively. The C 1s signal decreased from ~18% to <5%, confirming the gradual removal of surface carbon. After annealing, F was significantly reduced (<2% throughout), while the Ti content increased to ~59% and O to ~38%, demonstrating oxide densification and improved stoichiometry. These changes affirm that annealing enhances the anodic oxide's chemical purity and structural stability by eliminating fluorinated species that could otherwise act as corrosion initiators.

Taken together, the XRD, SEM-EDS, and XPS results provide a comprehensive view of the evolution of the TiO_2 surface layer during anodization and annealing. The oxide film exhibits desirable characteristics, anatase crystallinity, porous morphology, homogeneous composition, and low impurity levels, all of which support the improved corrosion resistance demonstrated in subsequent electrochemical studies.[16,21] The removal of fluoride residues and reduction of carbon content upon annealing are particularly crucial in enhancing long-term performance in oxidizing aqueous environments such as H_2O_2 containing electrolytes.

Corrosion behavior and electrochemical analysis

The open circuit potential (OCP) measurements provide an initial indication of the thermodynamic stability of the oxide layer in different environments (Fig. 6). Bare Ti displayed relatively stable OCP values across all H_2O_2 concentrations, ranging from 467 to 496 mV *vs.* Ag/AgCl. However, the slight drop in the OCP at 0.1 M H_2O_2 reflects increasing oxidative dissolution of the native oxide film. Anodized Ti, on the other hand, exhibited more negative OCP values at low H_2O_2 concentrations (*e.g.*, −352 mV at 0.01 M concentration), followed by a progressive

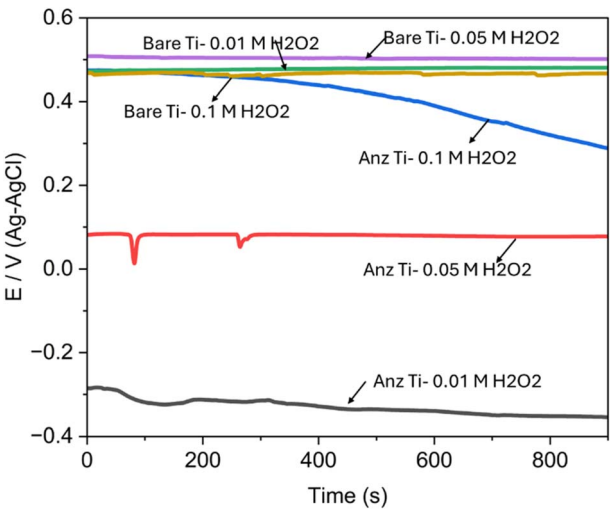

Fig. 6 Open circuit potential (OCP) evolution of bare and anodized Ti samples in 25 mM Na_2SO_4 with increasing H_2O_2 concentrations (0–0.1 M). Bare Ti shows relatively stable OCP values with slight negative shifts at higher peroxide contents. At the same time, anodized Ti initially exhibits more negative OCP but progressively shifts to positive potentials at higher H_2O_2, indicating adaptive passivation of the anodic oxide layer.

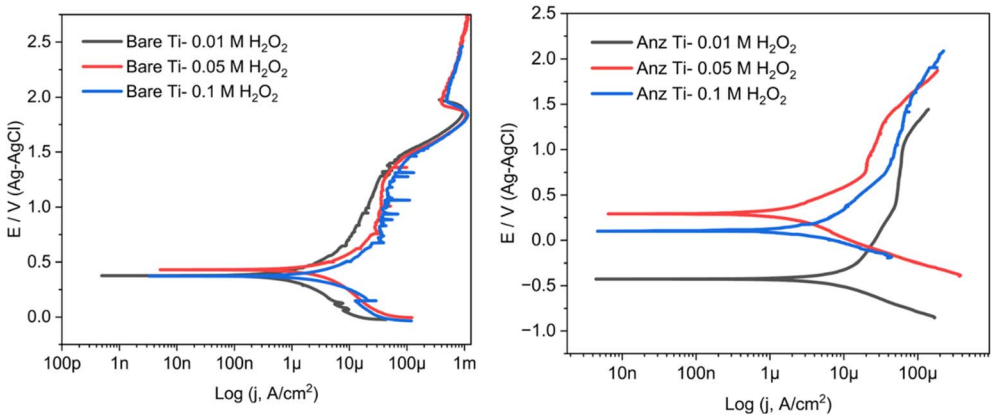

Fig. 7 Potentiodynamic polarization curves of bare and anodized Ti samples in 25 mM Na_2SO_4 with increasing amount of H_2O_2. Anodized Ti shows significantly lower corrosion current densities (I_{corr}) and more stable passive regions than bare Ti. The anodic and cathodic Tafel slopes highlight improved barrier properties of the anodized oxide, particularly after annealing, under oxidizing conditions.

Table 1 Tafel extrapolation data for bare and anodized titanium in 25 mM Na_2SO_4 with varying H_2O_2 concentrations in deionized water, showing corrosion potential (E_{corr}), corrosion current density (I_{corr}), anodic and cathodic Tafel slopes (β_a and β_c), and calculated corrosion rates

	25 mM Na_2SO_4 + x M H_2O_2 in DI water	E_{corr} (mV)	I_{corr} (μA cm^{-2})	β_a (mV dec^{-1})	β_c (mV dec^{-1})	Corrosion rate (mmpy)
Bare Ti	0.01 M H_2O_2	378	1.43	321	388	12.32×10^{-3}
Bare Ti	0.05 M H_2O_2	432	6.66	479	653	57.45×10^{-3}
Bare Ti	0.1 M H_2O_2	374	4.44	359	289	38.23×10^{-3}
Anodized Ti	0.01 M H_2O_2	−425	3.96	182	160	34.19×10^{-3}
Anodized Ti	0.05 M H_2O_2	292	2.66	513	419	22.94×10^{-3}
Anodized Ti	0.1 M H_2O_2	101	2.32	475	218	20.08×10^{-3}

increase in the OCP with increasing H_2O_2. At 0.1 M H_2O_2, the OCP reached +289 mV, indicating that the anodized and annealed Ti surface can rapidly adapt to oxidizing conditions by reforming or restructuring the protective oxide. This adaptive behavior is attributed to the enhanced redox activity of the anodic oxide and the improved chemical purity following fluoride removal, as confirmed by XPS analysis.

Potentiodynamic polarization (Fig. 7) provides further insight into corrosion kinetics and passive film breakdown under oxidative stress. Bare Ti samples showed increasing corrosion current density (I_{corr}) with increasing H_2O_2 concentration, increasing from 1.43 μA at 0.01 M concentration to 6.66 μA at 0.05 M H_2O_2. The corresponding corrosion rates nearly quintupled, reflecting the progressive loss of passive film protection.

Notably, the anodic Tafel slopes (β_a) also changed significantly with environmental and surface conditions (Table 1). For bare Ti, β_a increased from 321 mV dec^{-1} to 479 mV dec^{-1} with increasing peroxide concentration, indicating more sluggish electron transfer kinetics as oxide instability promotes non-uniform corrosion paths. The cathodic slopes (β_c) followed a similar trend, increasing from 388 to 653 mV dec^{-1}, which may be associated with increased oxygen evolution reaction (OER) activity at higher potentials.

In anodized Ti, the I_{corr} values remained significantly lower, and corrosion rates were consistently suppressed. The anodic slopes ranged from 182 to 475 mV dec^{-1} and cathodic slopes from 160 to 418 mV dec^{-1}, suggesting that the anodic oxide provides a more stable and uniform electrochemical interface. At 0.1 M H_2O_2, the anodized sample showed the highest β_a, which may reflect enhanced resistive barrier properties and a more compact oxide structure. These observations are consistent with the XPS results, where annealed oxides were shown to be fluorine free and chemically dense.

The higher anodic slopes in anodized Ti samples under peroxide-rich conditions may also indicate a suppression of localized dissolution, with current being carried primarily through oxygen evolution rather than metal ion release. This distinction highlights the role of oxide purity and structure in resisting chemical dissolution. The known reaction of TiO_2 with H_2O_2, forming soluble peroxotitanium complexes, follows the equation:

$$TiO_2 + H_2O_2 + 2H^+ \rightarrow [TiO_2(O_2)] + H_2O \quad (1)$$

This mechanism dominates in bare and anodized Ti, where fluoride inclusion facilitates oxide dissolution. In anodized and annealed Ti, such reactions are greatly mitigated due to the absence of fluoride (as shown in XPS depth profiling) and a more compact, crystalline anatase structure (confirmed by XRD).

Electrochemical impedance spectroscopy (EIS)

Electrochemical impedance spectroscopy was employed to assess the electrochemical behavior of bare and anodized Ti samples

exposed to varying concentrations of H_2O_2 in a 25 mM Na_2SO_4 solution. The Nyquist and Bode plots (Fig. 8) were modeled using a constant phase element (CPE)-based equivalent circuit, and fitted parameters are presented in Table 2. The extracted values include the solution resistance (R_u), polarization resistance (R_p), CPE admittance (Y_0), and phase exponent (α).

In this study, the polarization resistance (R_p) was determined from the EIS data as the difference between the low-frequency and high-frequency intercepts of the Nyquist plot on the real axis, corresponding to the semicircle diameter. It is important to note that R_p values obtained from EIS may differ from those derived *via* the Stern–Geary equation using polarization curves, since the former captures frequency-dependent interfacial impedance behavior, whereas the latter is based on polarization kinetics. For bare titanium, the EIS response reveals large semicircular arcs in the Nyquist plots, especially for 0.01 M and 0.05 M H_2O_2, suggesting a high charge transfer resistance and a well-formed passive film. The R_p values were the highest at 0.01 M H_2O_2 (1.52×10^4 Ω cm^2), gradually decreasing with increasing H_2O_2 concentration, reaching 5.47×10^3 Ω cm^2 at 0.1 M concentration. This trend reflects the onset of passive film instability at higher oxidizer concentrations, where aggressive oxidative species such as $HO^{\bullet}$ and O_2 may contribute to oxide dissolution or destabilization of surface states.

In contrast, anodized Ti exhibited lower R_p values across all H_2O_2 concentrations, with the lowest being 321.3 Ω cm^2 at 0.05 M concentration. At first glance, this might suggest a decline in corrosion resistance after anodization. However, this interpretation would be misleading if based solely on R_p. Anodized Ti surfaces are characterized by a porous TiO_2 layer (confirmed by SEM and XRD), which introduces a high surface area and an open network for electrolyte interactions. Such nanostructured films often promote higher electrochemical activity without compromising the overall protective behavior.

Additionally, the CPE parameters (Y_0 and α) further support this interpretation. Anodized Ti shows lower Y_0 values (*e.g.*, 1.55×10^{-5} S s^n cm^{-2} at 0.05 M H_2O_2), reflecting a more resistive interface, possibly due to thicker oxide or reduced porosity after annealing. The α values were in the range of 0.80–0.89, indicating nearly ideal capacitive behavior for both bare and anodized samples. Notably, anodized Ti at 0.05 M H_2O_2 exhibited $\alpha \approx 0.88$, suggesting a more homogeneous and dielectric-like oxide structure. These characteristics align with the presence of well-ordered, compact oxides that resist degradation in oxidizing environments.

The Bode phase plots reinforce this trend, with broader phase angle peaks in bare Ti, signifying slower time constants, while anodized Ti shows shifts to higher frequencies, indicating more electroactive but still stable behavior.[20,26] This can be attributed to surface reactions occurring within the nanoporous oxide layer rather than at the bulk metal interface, further distinguishing the corrosion protection mechanism.[7]

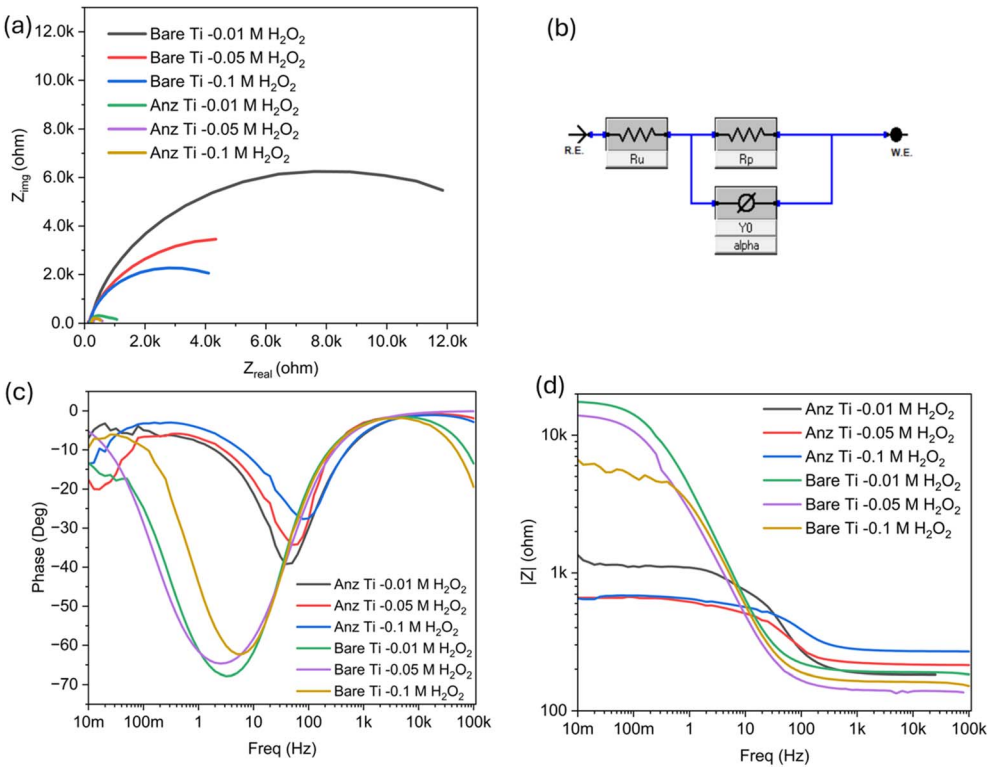

Fig. 8 Electrochemical impedance spectroscopy (EIS) of bare and anodized Ti in 25 mM Na_2SO_4 with increasing H_2O_2 concentrations (0.01–0.1 M). (a) Nyquist plots, (b) equivalent circuit model (R_u–R_p–CPE) used for fitting the spectra, (c) Bode magnitude plots, and (d) Bode phase plots. Bare Ti at 0.01 M H_2O_2 shows the most immense semicircle and the highest R_p, but this protection rapidly decreases at higher peroxide levels. Anodized Ti, although showing smaller R_p values initially, exhibits more stable low-frequency impedance and consistent α values, indicating a more uniform porous oxide film with improved adaptability under oxidizing conditions.

Table 2 Electrochemical impedance spectroscopy (EIS) parameters for bare and anodized titanium in 25 mM Na_2SO_4 with varying H_2O_2 concentrations. R_p: polarization resistance; R_u: solution resistance; Y_0 and α: constant phase element (CPE) parameters; values obtained from fitted equivalent circuit modeling

	25 mM Na_2SO_4 + x M H_2O_2 in DI water	R_p (Ω cm^2)	R_u (Ω cm^2)	Y_0	α	Fitting error (χ^2)
Bare	0.01 M H_2O_2	1.52×10^4	186.3	4.77×10^{-5}	8.07×10^{-1}	2.40×10^{-3}
Bare	0.05 M H_2O_2	1.40×10^4	137.8	7.21×10^{-5}	8.36×10^{-1}	1.44×10^{-2}
Bare	0.1 M H_2O_2	5.47×10^3	160.7	4.80×10^{-5}	8.65×10^{-1}	7.03×10^{-3}
Anodized Ti	0.01 M H_2O_2	950.4	179.5	3.29×10^{-5}	8.20×10^{-1}	4.07×10^{-3}
Anodized Ti	0.05 M H_2O_2	321.3	216.1	1.55×10^{-5}	8.88×10^{-1}	1.41×10^{-2}
Anodized Ti	0.1 M H_2O_2	391.9	264.2	2.83×10^{-5}	8.25×10^{-1}	8.26×10^{-3}

It is therefore important to emphasize that the lower R_p in anodized samples does not imply inferior protection. Instead, the oxide structure allows for controlled electrochemical interactions, possibly facilitating reactions such as oxygen evolution or H_2O_2 decomposition within the oxide network, while maintaining film integrity. This is consistent with XPS results, showing the removal of fluoride species, a stable Ti–O framework post-annealing, and XRD confirmation of the crystalline anatase TiO_2 phase.

In summary, EIS results reveal that bare Ti demonstrates higher impedance due to its compact but thinner native oxide, which becomes increasingly vulnerable at high H_2O_2 concentrations. Anodized Ti, although exhibiting lower R_p, maintains superior chemical stability due to its structured and chemically inert oxide layer. This highlights the importance of interpreting EIS with Tafel, XPS, and morphological data for a holistic understanding of corrosion behavior.

Conclusions

This study successfully fabricated highly ordered nanoporous titanium dioxide (TiO_2) layers *via* optimized anodization and thermal annealing to enhance corrosion resistance in oxidizing environments. The resulting structures featured uniform pores (60–70 nm) and 2–3 μm thicknesses, with crystallization into the anatase phase, as confirmed by XRD.

XPS depth profiling demonstrated the effective removal of fluorine and surface contaminants after annealing, resulting in chemically pure and stable oxide layers. Electrochemical analysis revealed that anodized Ti exhibited significantly lower corrosion current densities and more stable passivation at increasing H_2O_2 concentrations than bare Ti. Although the anodized samples showed lower polarization resistance (R_p) in EIS, this was attributed to increased interfacial activity within the nanoporous structure rather than oxide degradation. Tafel and EIS results confirmed the protective and adaptive nature of the anodic oxide under oxidative stress when interpreted in conjunction with surface analysis.

These findings highlight the importance of structural control and post-treatment in tailoring TiO_2 films for long-term durability in harsh environments. The integrated approach demonstrated here provides a robust pathway for advancing titanium-based materials in biomedical implants, catalytic systems, and nuclear coolant loop components. Future work will focus on long-term durability, scaling anodization processes for industrial applications, and corrosion performance under irradiation or complex mechanical loads.

Conflicts of interest

There are no conflicts to declare.

Data availability

The data supporting the findings of this study are available within the article. Additional raw data, including SEM images, XRD profiles, and electrochemical test files, can be provided by the corresponding author upon reasonable request.

Supplementary information is available. See DOI: https://doi.org/10.1039/d5na00883b.

Acknowledgements

This research was carried out by the Emirates Nuclear Technology Centre, a collaboration among Khalifa University of Science and Technology, Emirates Nuclear Energy Company, and the Federal Authority for Nuclear Regulation.

Notes and references

1 Q. Zhou, M. Tian, Z. Ying, Y. Dan, F. Tang, J. Zhang, *et al.*, Dense films formed during Ti anodization in NH4F electrolyte: Evidence against the field-assisted dissolution reactions of fluoride ions, *Electrochem. Commun.*, 2020, **111**, 106663. https://consensus.app/papers/dense-films-formed-anodization-nh4f-electrolyte-evidence-zhou/05156053b44d58d5a7f9704a35b8ddd4/.

2 X. Zhou, N. Nguyen, S. Ozkan and P. Schmuki, Anodic TiO2 nanotube layers: Why does self-organized growth occur—A mini review, *Electrochem. Commun.*, 2014, **46**, 157–162. https://consensus.app/papers/anodic-tio2-nanotube-layers-selforganized-growth-occur—a-zhou/e7342a7696d85082a2bfdc43fb80f76b/.

3 C. Yao and T. J. Webster, Anodization: a promising nano-modification technique of titanium implants for orthopedic applications, *J. Nanosci. Nanotechnol.*, 2006, **6**(9–10), 2682–2692, DOI: 10.1166/jnn.2006.447.

4 M. Momeni and M. Motalebian, Chromium-doped titanium oxide nanotubes grown via one-step anodization for efficient photocathodic protection of stainless steel, *Surf. Coat. Technol.*, 2021, **420**, 127304. https://consensus.app/papers/chromiumdoped-titanium-oxide-nanotubes-onestep-momeni/78bea1195c125ed3a47c8d8bb80e5be2/.

5 S. Jain, R. Scott Williamson and M. D. Roach, Surface characterization, shear strength, and bioactivity of anodized titanium prepared in mixed-acid electrolytes, *Surf. Coat. Technol.*, 2017, **325**, 594–603, DOI: 10.1016/j.surfcoat.2017.07.010.

6 Z. Yang, Y. Gong and J. Yuan, Failure analysis of leakage on titanium tubes within heat exchangers in a nuclear power plant. part i: electrochemical corrosion, *Mater. Corros.*, 2011, **63**(1), 7–17, DOI: 10.1002/maco.201106189.

7 M. V. Diamanti, M. Ormellese and M. Pedeferri, Application-wise nanostructuring of anodic films on titanium: a review, *J. Exp. Nanosci.*, 2015, **10**(17), 1285–1308, DOI: 10.1080/17458080.2014.999261.

8 B. D. Mohapatra and G. D. Sulka, Review of Anodic Tantalum Oxide Nanostructures: From Morphological Design to Emerging Applications, *ACS Appl. Nano Mater.*, 2024, **7**(12), 13865–13892, DOI: 10.1021/acsanm.4c02000.

9 H. Kim and K. H. Lee, Dependence of the Morphology of Nanostructured Titanium Oxide on Fluoride Ion Content, *Electrochem. Solid-State Lett.*, 2009, **12**(3), C10, DOI: 10.1149/1.3054324.

10 A. K. Sharma, Anodizing titanium for space applications, *Thin Solid Films*, 1992, **208**(1), 48–54, DOI: 10.1016/0040-6090(92)90946-9.

11 S. Minagar, C. Berndt and C. Wen, Fabrication and Characterization of Nanoporous Niobia, and Nanotubular Tantala, Titania and Zirconia via Anodization, *J. Funct. Biomater.*, 2015, **6**, 153–170. https://consensus.app/papers/fabrication-characterization-nanoporous-niobia-minagar/58f40b640fec5553bec088a09024f190/.

12 K. Huo, B. Gao, J. Fu, L. Zhao and P. K. Chu, Fabrication, modification, and biomedical applications of anodized TiO 2 nanotube arrays, *RSC Adv.*, 2014, **4**(33), 17300–17324, DOI: 10.1039/C4RA01458H.

13 A. Ravoiu, N. Simionescu and L. Benea, Influence of different concentration of hydrogen peroxide on the corrosion behavior of Ti-6Al-4V alloy immersed in physiological solution, *IOP Conf. Ser.: Mater. Sci. Eng.*, 2019, **572**(1), 012006, DOI: 10.1088/1757-899X/572/1/012006.

14 C. Fonseca and M. A. Barbosa, Corrosion behaviour of titanium in biofluids containing H2O2 studied by electrochemical impedance spectroscopy, *Corros. Sci.*, 2001, **43**(3), 547–559. https://www.sciencedirect.com/science/article/pii/S0010938X00001074.

15 S. Karuppuchamy, J. M. Jeong, D. Amalnerkar and H. Minoura, Photoinduced hydrophilicity of titanium dioxide thin films prepared by cathodic electrodeposition, *Vacuum*, 2006, **80**, 494–498. https://consensus.app/papers/photoinduced-hydrophilicity-of-titanium-dioxide-thin-karuppuchamy-jeong/b3ea8d096836551d88acda44387c8bd2/.

16 A. Alves, F. Wenger, P. Ponthiaux, J. Celis, A. Pinto, L. Rocha, *et al.*, Corrosion mechanisms in titanium oxide-based films produced by anodic treatment, *Electrochim. Acta*, 2017, **234**, 16–27. https://consensus.app/papers/corrosion-mechanisms-titanium-oxidebased-films-produced-alves/f586a13a437c552c81b285fcd0f6dbd4/.

17 D. Regonini, C. R. Bowen, A. Jaroenworaluck and R. Stevens, A review of growth mechanism, structure and crystallinity of anodized TiO2 nanotubes, *Mater. Sci. Eng., R*, 2013, **74**(12), 377–406, DOI: 10.1016/j.mser.2013.10.001.

18 J. Kapusta-Kołodziej, A. Chudecka and G. D. Sulka, 3D nanoporous titania formed by anodization as a promising photoelectrode material, *J. Electroanal. Chem.*, 2018, **823**, 221–233, DOI: 10.1016/j.jelechem.2018.06.014.

19 J. Grotberg, A. Hamlekhan, A. Butt, S. B. Patel, D. Royhman, T. Shokuhfar, *et al.*, Thermally oxidized titania nanotubes enhance the corrosion resistance of Ti6Al4V, *Mater. Sci. Eng., C*, 2016, **59**, 677–689. https://consensus.app/papers/thermally-oxidized-titania-nanotubes-enhance-corrosion-grotberg/004d28527262566a92133022cda9beb3/.

20 P. L. Chen, C. T. Kuo, T. G. Tsai, B. W. Wu, C. C. Hsu and F. M. Pan, Self-organized titanium oxide nanodot arrays by electrochemical anodization, *Appl. Phys. Lett.*, 2003, **82**(17), 2796–2798, DOI: 10.1063/1.1571661.

21 J. Yi, M. Li, J. Zhu, Z. Wang and X. Li, Recent development and applications of electrodeposition biocoatings on medical titanium for bone repair, *J. Mater. Chem. B*, 2024, **12**(39), 9863–9893, DOI: 10.1039/d4tb01081g.

22 E. Afshoon, S. Asadi, S. Lashgari and M. Shanbedi, From surface to structure: The role of preparation techniques in shaping titanium dioxide nanotubes via anodization, *Ceram. Interfaces*, 2025, **51**(6), 6985–6992, DOI: 10.1016/j.ceramint.2024.12.133.

23 M. Otadi, E. Borhani and S. Faghihi, Combined bulk nanostructuring and surface modifications of titanium substrate for improved corrosion behavior, *Surf. Coat. Technol.*, 2024, **493**, 131229. https://www.sciencedirect.com/science/article/pii/S0257897224008600.

24 H. Dhiflaoui, W. Zayani, Y. Dabaki, M. A. Hajjaji, A. Bessadok-Jemai, L. Khezami, *et al.*, Corrosion Study of TiO2 Nanotubes Decorated with Ag Silver Nanoparticles Prepared by Photoreduction Process, *J. Mater. Eng. Perform.*, 2025, **34**(15), 16230–16243, DOI: 10.1007/s11665-024-10326-8.

25 Q. Rao, J. Zhang, Y. Chen, Y. Yang, X. Chen, D. Liu, *et al.*, Research Progress of the Coatings Fabricated onto Titanium and/or Titanium Alloy Surfaces in Biomaterials for Medical Applications for Anticorrosive Applications, *Coatings*, 2025, **15**(5), 599, DOI: 10.3390/coatings15050599.

26 A. B. Stoian, M. Vardaki, D. Ionita, M. Enachescu, M. Prodana, O. Brancoveanu, *et al.*, Nanopores and nanotubes ceramic oxides elaborated on titanium alloy with zirconium by changing anodization potentials, *Ceram. Int.*, 2018, **44**(6), 7026–7033, DOI: 10.1016/j.ceramint.2018.01.137.